Supporting information for: DFT Investigation on the Adsorption of Munition Compounds on α-Fe_2O_3: Similarity and Differences with α-Al_2O_3

Glen R. Jenness,* Jennifer Seiter, and Manoj K. Shukla*

Environmental Laboratory, US Army Engineer Research and Development Center, 3909 Halls Ferry Road, Vicksburg, Mississippi 39180, United States

E-mail: Glen.R.Jenness@usace.army.mil; Manoj.K.Shukla@usace.army.mil

Table S1: Binding energy comparison between the number of stoichiometric layers for TNT on α-Fe_2O_3 (0001). Units in eV.

Structure Index	3 layer	6 layer	ΔE_{BE}
Flat 0	−1.81	−1.88	0.07
Flat 1	−1.75	−1.82	0.07
Flat 2	−1.79	−1.68	0.12
Flat 3	−1.69	−1.77	0.07
Flat 4	−1.71	−1.75	0.04

Table S2: Mean binding energies and standard deviations for the munition compounds in Figure 3 of the main text on the α-Al_2O_3 (0001) and α-Fe_2O_3 (0001) surfaces (units in eV).

Molecule	Binding mode	α-Fe_2O_3 (0001)	α-Al_2O_3 (0001)
	Mode 1	−2.53±0.05	−1.68±0.06
TNT	Mode 2	−2.53±0.09	−1.63±0.06
	Flat	−3.05±0.12	−1.76±0.07
	Mode 1	−2.36±0.08	−1.61±0.07
DNAN	Mode 2	−2.32±0.08	−1.62±0.06
	Flat	−2.60±0.29	−2.03±0.32
	Mode 1	−2.85±0.18	−2.08±0.09
NTO	Mode 2	−2.22±0.05	−1.31±0.09
	Flat	−3.40±0.49	−1.97±0.28
	Mode 1	−2.47±0.07	−1.71±0.08
NQ	Mode 2	−2.73±0.11	−1.95±0.42
	Flat	−2.54±0.24	−1.65±0.12

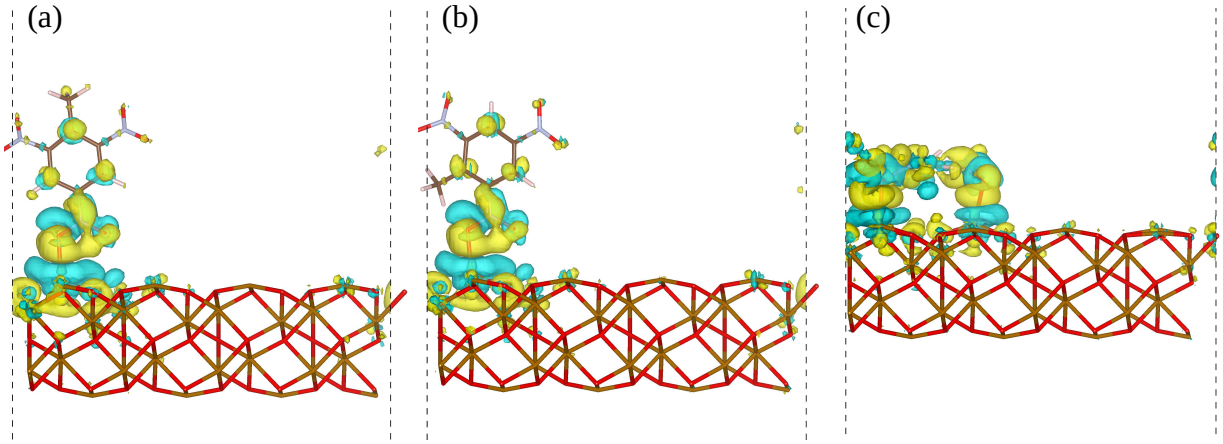

Figure S1: Charge density differences (ρ_{diff}) for TNT on the α-Fe_2O_3 (0001) surface. Yellow regions denote areas of charge accumulation whilst blue regions denotes areas of charge depletion.

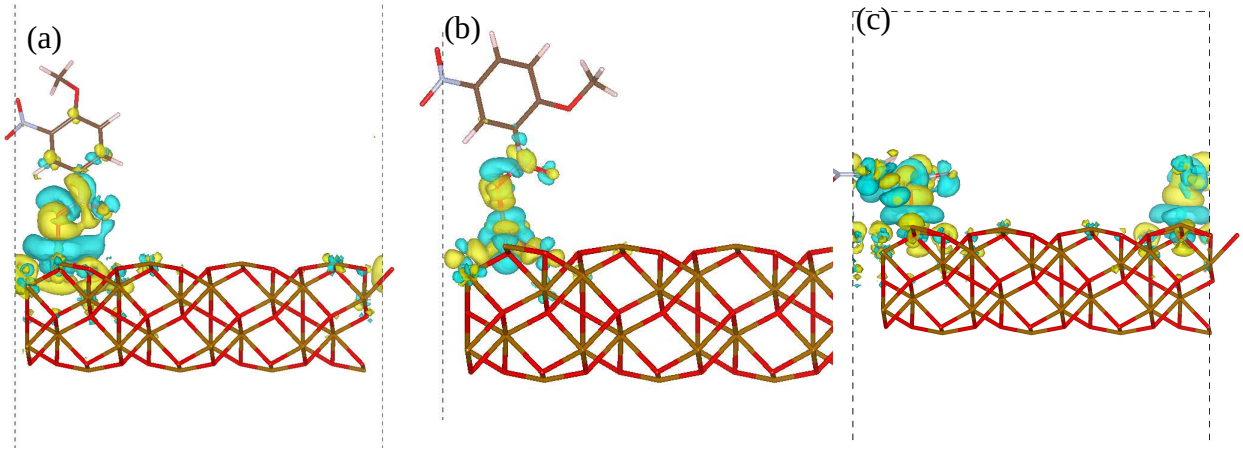

Figure S2: Charge density differences (ρ_{diff}) for DNAN on the α-Fe_2O_3 (0001) surface. Yellow regions denote areas of charge accumulation whilst blue regions denotes areas of charge depletion.

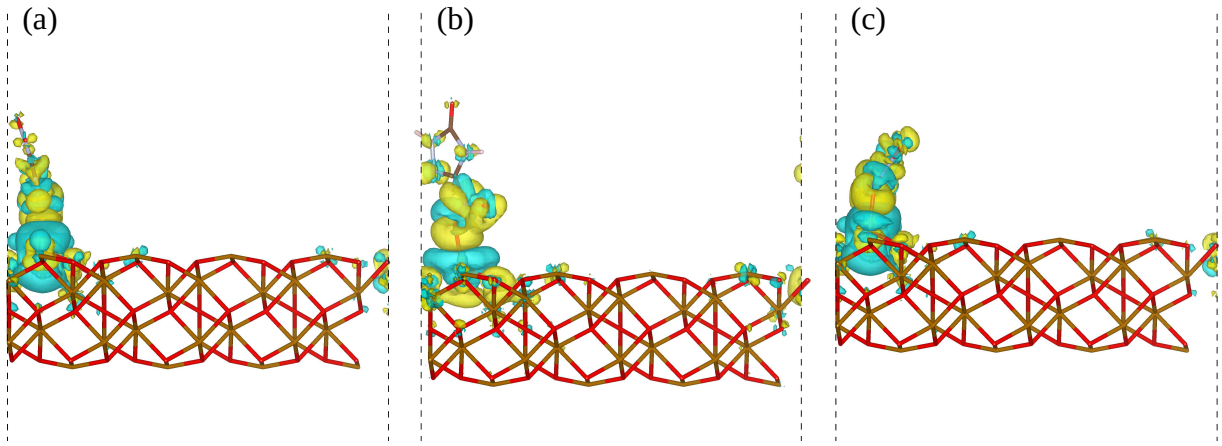

Figure S3: Charge density differences (ρ_{diff}) for NTO on the α-Fe_2O_3 (0001) surface. Yellow regions denote areas of charge accumulation whilst blue regions denotes areas of charge depletion.

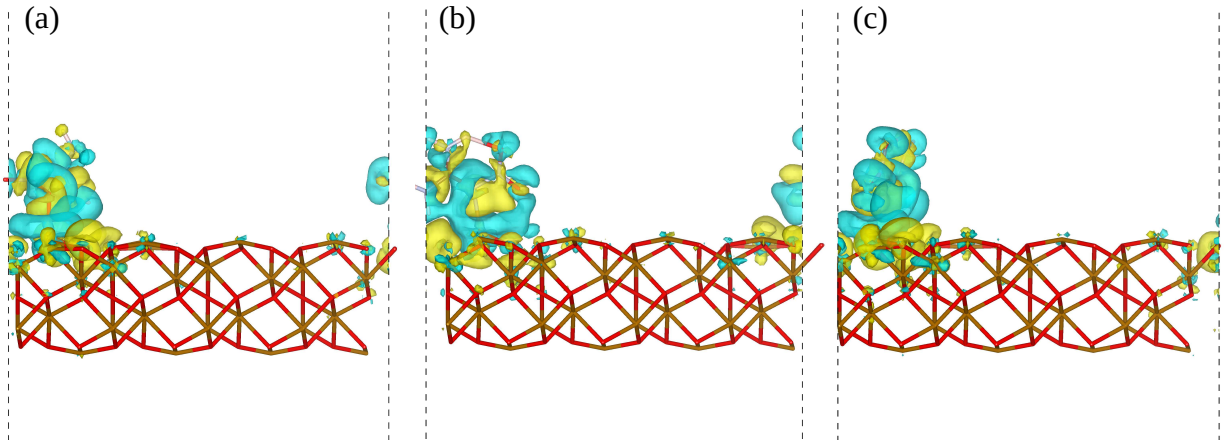

Figure S4: Charge density differences (ρ_{diff}) for NQ on the α-Fe_2O_3 (0001) surface. Yellow regions denote areas of charge accumulation whilst blue regions denotes areas of charge depletion.

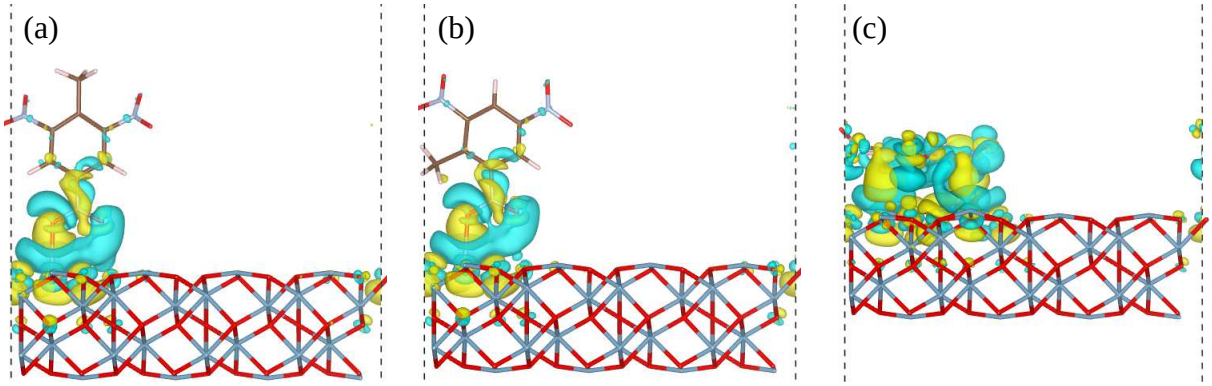

Figure S5: Charge density differences (ρ_{diff}) for TNT on the α-Al_2O_3 (0001) surface. Yellow regions denote areas of charge accumulation whilst blue regions denotes areas of charge depletion.

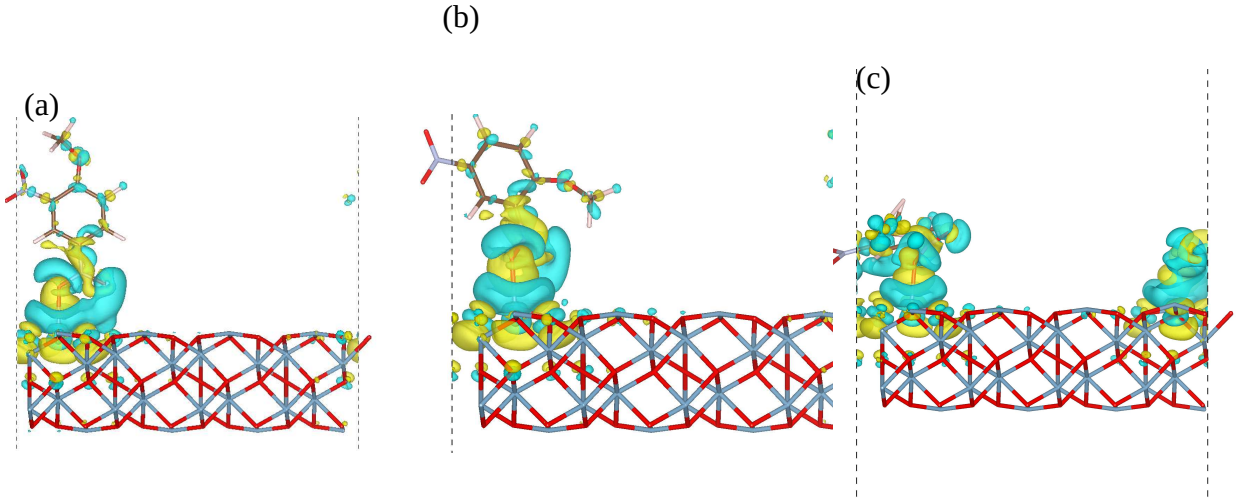

Figure S6: Charge density differences (ρ_{diff}) for DNAN on the α-Al_2O_3 (0001) surface. Yellow regions denote areas of charge accumulation whilst blue regions denotes areas of charge depletion.

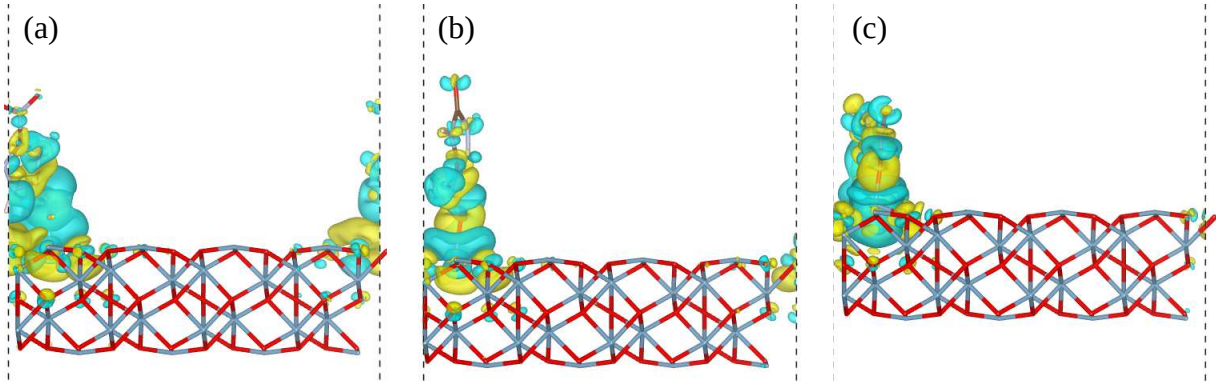

Figure S7: Charge density differences (ρ_{diff}) for NTO on the α-Al_2O_3 (0001) surface. Yellow regions denote areas of charge accumulation whilst blue regions denotes areas of charge depletion.

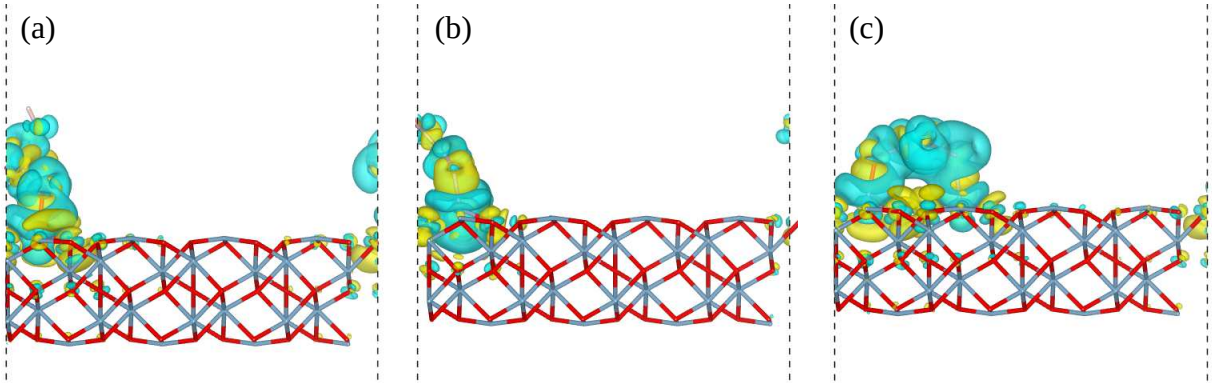

Figure S8: Charge density differences (ρ_{diff}) for NQ on the α-Al_2O_3 (0001) surface. Yellow regions denote areas of charge accumulation whilst blue regions denotes areas of charge depletion.

Table S3: Bond lengths and percent bond changes for DNAN in the gas-phase and on the soil oxide surfaces in the mode 1 binding mode. Units in Å.

Bond	Gas-Phase	α-Fe_2O_3 (0001)		α-Al_2O_3 (0001)	
		Bond Length	% Change	Bond Length	% Change
H0-C1	1.089	1.088	−0.089	1.088	−0.047
C1-C2	1.397	1.393	−0.247	1.393	−0.234
C1-C10	1.387	1.394	0.535	1.390	0.187
C2-N3	1.475	1.477	0.096	1.476	0.047
C2-C4	1.417	1.420	0.195	1.421	0.273
N3-O12	1.231	1.229	−0.154	1.228	−0.251
N3-O13	1.234	1.234	0.043	1.233	−0.102
C4-O5	1.344	1.342	−0.162	1.337	−0.497
C4-C6	1.411	1.413	0.124	1.414	0.234
O5-C16	1.442	1.439	−0.195	1.443	0.057
C6-H7	1.090	1.089	−0.025	1.089	−0.041
C6-C8	1.382	1.378	−0.281	1.376	−0.418
C8-H9	1.088	1.088	−0.059	1.088	−0.005
C8-C10	1.400	1.404	0.347	1.404	0.335
C10-N11	1.478	1.434	−3.080	1.441	−2.559
N11-O14	1.231	1.289	4.458	1.279	3.756
N11-O15	1.232	1.226	−0.503	1.216	−1.296
C16-H17	1.095	1.094	−0.087	1.095	−0.073
C16-H18	1.096	1.095	−0.131	1.098	0.187
C16-H19	1.099	1.099	0.016	1.095	−0.403

Table S4: Bond lengths and percent bond changes for DNAN in the gas-phase and on the soil oxide surfaces in the mode 2 binding mode. Units in Å.

Bond	Gas-Phase	α-Fe_2O_3 (0001)		α-Al_2O_3 (0001)	
		Bond Length	% Change	Bond Length	% Change
H0-C1	1.089	1.086	−0.233	1.088	−0.104
C1-C2	1.397	1.397	0.064	1.401	0.309
C1-C10	1.387	1.385	−0.181	1.381	−0.445
C2-N3	1.475	1.431	−3.060	1.442	−2.282
C2-C4	1.417	1.433	1.125	1.426	0.651
N3-O12	1.231	1.288	4.442	1.276	3.536
N3-O13	1.234	1.228	−0.431	1.218	−1.333
C4-O5	1.344	1.340	−0.335	1.338	−0.430
C4-C6	1.411	1.409	−0.154	1.411	0.024
O5-C16	1.442	1.435	−0.445	1.441	−0.076
C6-H7	1.090	1.088	−0.160	1.090	0.027
C6-C8	1.382	1.388	0.460	1.381	−0.070
C8-H9	1.088	1.088	0.014	1.089	0.059
C8-C10	1.400	1.395	−0.311	1.402	0.194
C10-N11	1.478	1.474	−0.303	1.479	0.071
N11-O14	1.231	1.232	0.013	1.229	−0.200
N11-O15	1.232	1.231	−0.101	1.232	0.004
C16-H17	1.095	1.100	0.378	1.097	0.113
C16-H18	1.096	1.100	0.341	1.096	−0.022
C16-H19	1.099	1.093	−0.571	1.095	−0.357

Table S5: Bond lengths and percent bond changes for DNAN in the gas-phase and on the soil oxide surfaces in the flat binding mode. Units in Å.

Bond	Gas-Phase	α-Fe_2O_3 (0001)		α-Al_2O_3 (0001)	
		Bond Length	% Change	Bond Length	% Change
H0-C1	1.089	1.087	−0.182	1.088	−0.034
C1-C2	1.397	1.391	−0.403	1.395	−0.112
C1-C10	1.387	1.390	0.181	1.392	0.383
C2-N3	1.475	1.433	−2.976	1.454	−1.441
C2-C4	1.417	1.433	1.114	1.432	1.020
N3-O12	1.231	1.284	4.144	1.278	3.654
N3-O13	1.234	1.224	−0.832	1.210	−1.977
C4-O5	1.344	1.325	−1.413	1.329	−1.149
C4-C6	1.411	1.420	0.613	1.413	0.120
O5-C16	1.442	1.445	0.199	1.440	−0.116
C6-H7	1.090	1.088	−0.180	1.086	−0.367
C6-C8	1.382	1.396	1.025	1.380	−0.097
C8-H9	1.088	1.088	−0.059	1.089	0.057
C8-C10	1.400	1.399	−0.023	1.399	−0.010
C10-N11	1.478	1.430	−3.340	1.444	−2.356
N11-O14	1.231	1.279	3.731	1.271	3.132
N11-O15	1.232	1.226	−0.463	1.219	−1.053
C16-H17	1.095	1.099	0.363	1.099	0.323
C16-H18	1.096	1.100	0.382	1.093	−0.296
C16-H19	1.099	1.093	−0.589	1.099	−0.035

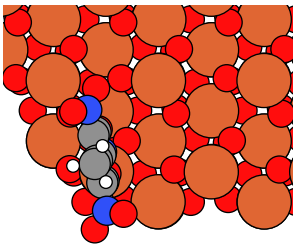

(a) Top view

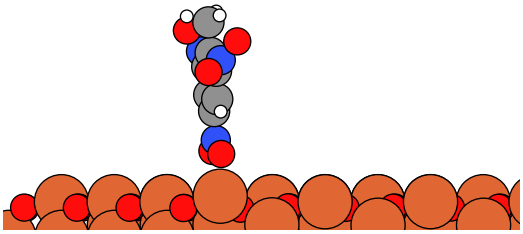

(b) Side view

Figure S9: Top (a) and side (b) views of TNT on α-Fe_2O_3 (0001) for binding mode 1, geometry #23

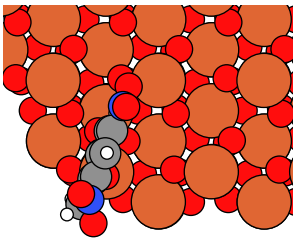

(a) Top view

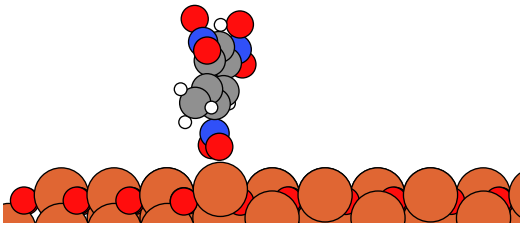

(b) Side view

Figure S10: Top (a) and side (b) views of TNT on α-Fe_2O_3 (0001) for binding mode 2, geometry #23

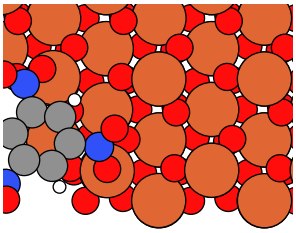

(a) Top view

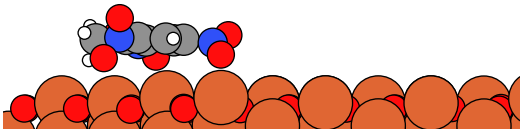

(b) Side view

Figure S11: Top (a) and side (b) views of TNT on α-Fe_2O_3 (0001) for binding mode flat, geometry #18

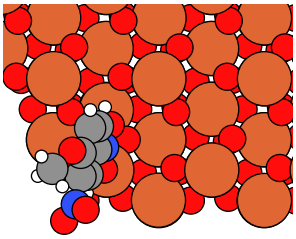

(a) Top view

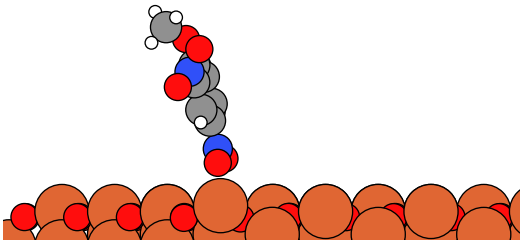

(b) Side view

Figure S12: Top (a) and side (b) views of DNAN on α-Fe_2O_3 (0001) for binding mode 1, geometry #24

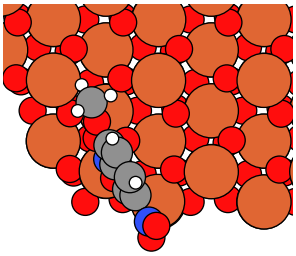

(a) Top view

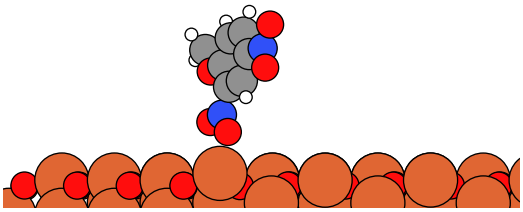

(b) Side view

Figure S13: Top (a) and side (b) views of DNAN on α-Fe_2O_3 (0001) for binding mode 2, geometry #21

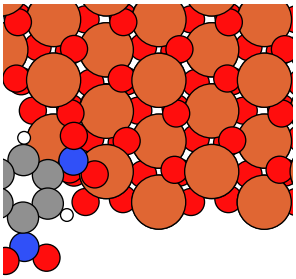

(a) Top view

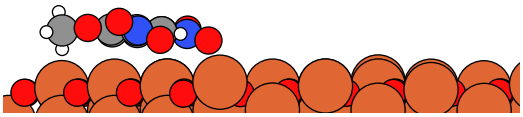

(b) Side view

Figure S14: Top (a) and side (b) views of DNAN on α-Fe_2O_3 (0001) for binding mode flat, geometry #21

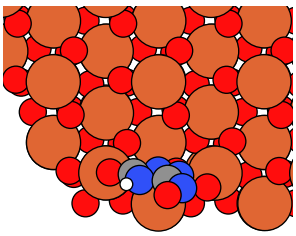

(a) Top view

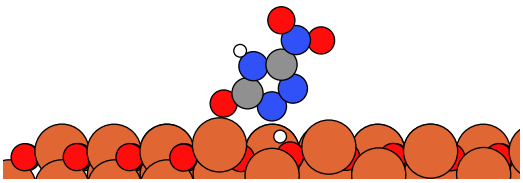

(b) Side view

Figure S15: Top (a) and side (b) views of NTO on α-Fe_2O_3 (0001) for binding mode 1, geometry #16

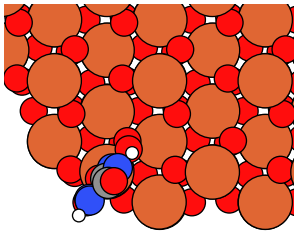

(a) Top view

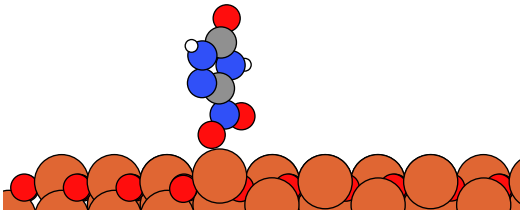

(b) Side view

Figure S16: Top (a) and side (b) views of NTO on α-Fe_2O_3 (0001) for binding mode 2, geometry #20

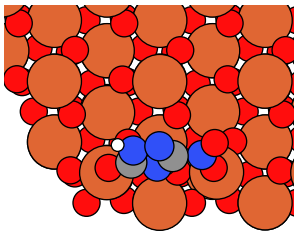

(a) Top view

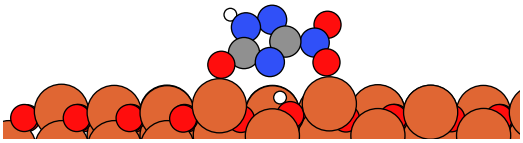

(b) Side view

Figure S17: Top (a) and side (b) views of NTO on α-Fe_2O_3 (0001) for binding mode flat, geometry #15

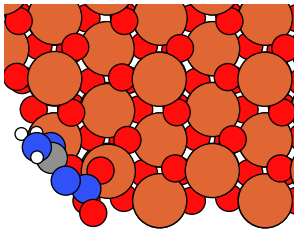

(a) Top view

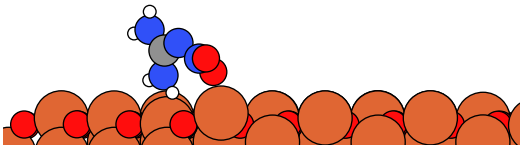

(b) Side view

Figure S18: Top (a) and side (b) views of NQ on α-Fe_2O_3 (0001) for binding mode 1, geometry #20

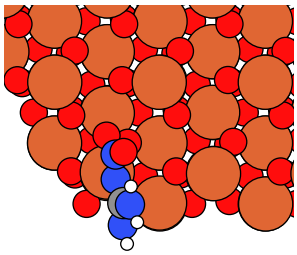

(a) Top view

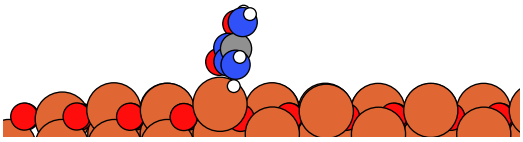

(b) Side view

Figure S19: Top (a) and side (b) views of NQ on α-Fe_2O_3 (0001) for binding mode 2, geometry #17

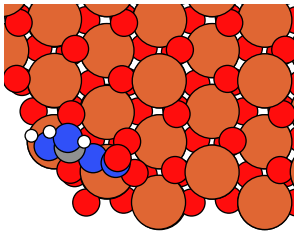

(a) Top view

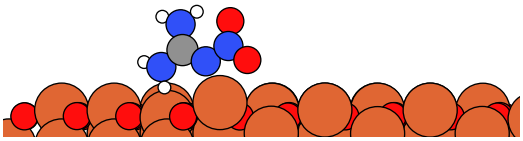

(b) Side view

Figure S20: Top (a) and side (b) views of NQ on α-Fe_2O_3 (0001) for binding mode flat, geometry #15

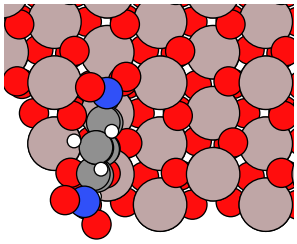

(a) Top view

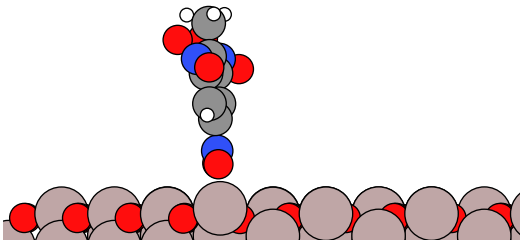

(b) Side view

Figure S21: Top (a) and side (b) views of TNT on α-Al_2O_3 (0001) for binding mode 1, geometry #22

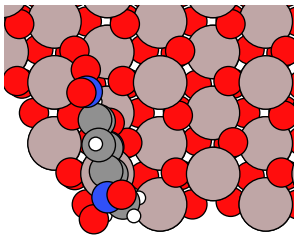

(a) Top view

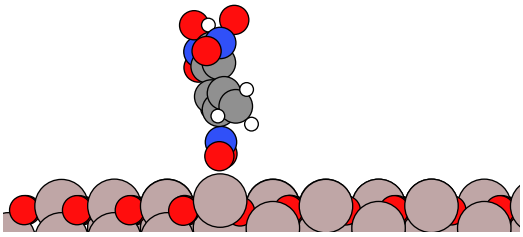

(b) Side view

Figure S22: Top (a) and side (b) views of TNT on α-Al_2O_3 (0001) for binding mode 2, geometry #21

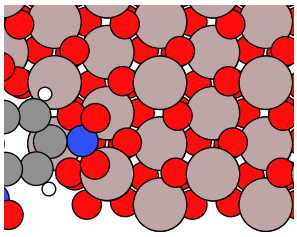

(a) Top view

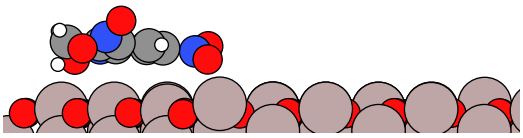

(b) Side view

Figure S23: Top (a) and side (b) views of TNT on α-Al_2O_3 (0001) for binding mode flat, geometry #18

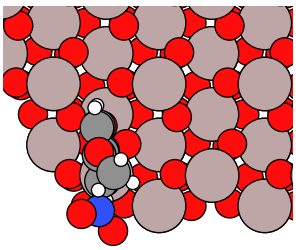

(a) Top view

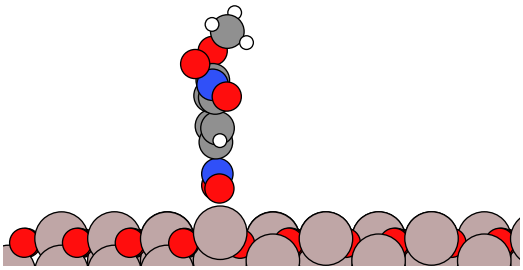

(b) Side view

Figure S24: Top (a) and side (b) views of DNAN on α-Al_2O_3 (0001) for binding mode 1, geometry #24

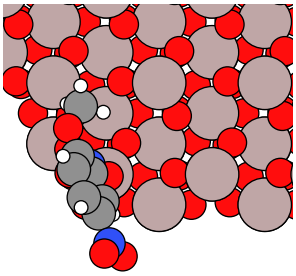

(a) Top view

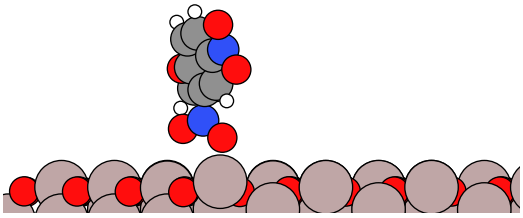

(b) Side view

Figure S25: Top (a) and side (b) views of DNAN on α-Al_2O_3 (0001) for binding mode 2, geometry #23

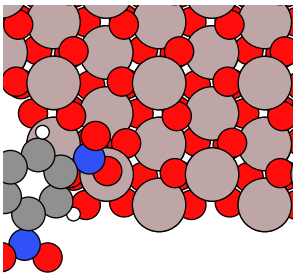

(a) Top view

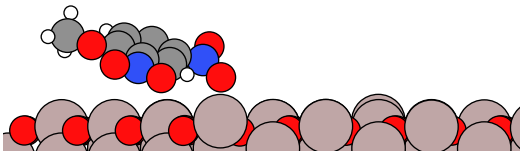

(b) Side view

Figure S26: Top (a) and side (b) views of DNAN on α-Al_2O_3 (0001) for binding mode flat, geometry #22

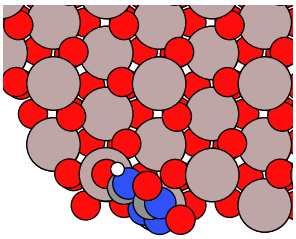

(a) Top view

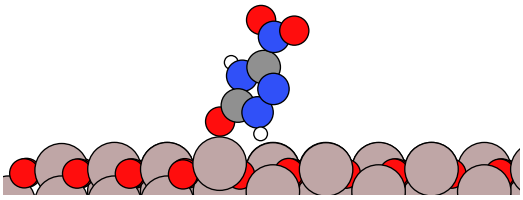

(b) Side view

Figure S27: Top (a) and side (b) views of NTO on α-Al_2O_3 (0001) for binding mode 1, geometry #17

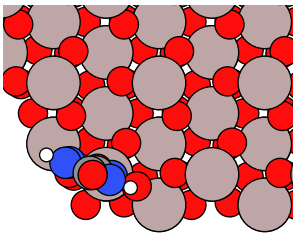

(a) Top view

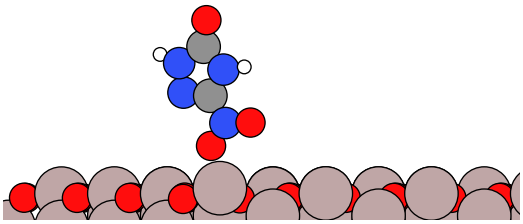

(b) Side view

Figure S28: Top (a) and side (b) views of NTO on α-Al_2O_3 (0001) for binding mode 2, geometry #21

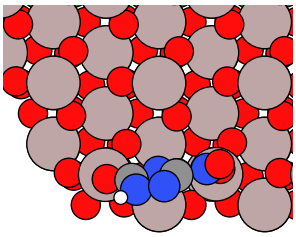

(a) Top view

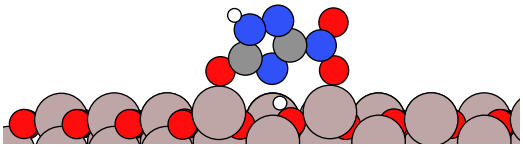

(b) Side view

Figure S29: Top (a) and side (b) views of NTO on α-Al_2O_3 (0001) for binding mode flat, geometry #20

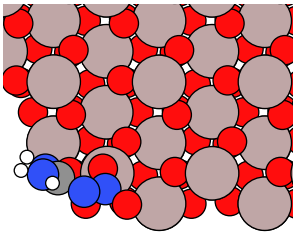

(a) Top view

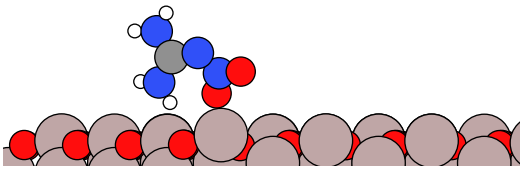

(b) Side view

Figure S30: Top (a) and side (b) views of NQ on α-Al_2O_3 (0001) for binding mode 1, geometry #18

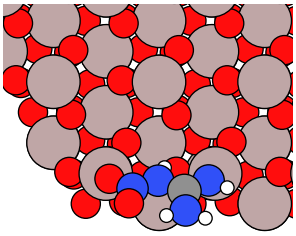

(a) Top view

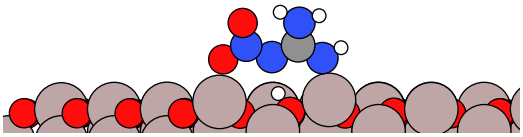

(b) Side view

Figure S31: Top (a) and side (b) views of NQ on α-Al_2O_3 (0001) for binding mode 2, geometry #17

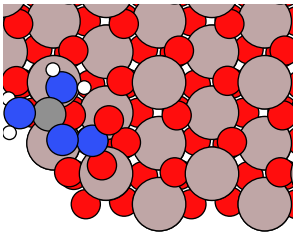

(a) Top view

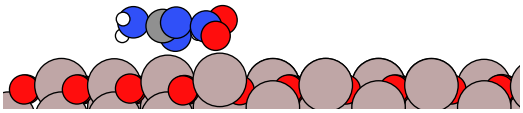

(b) Side view

Figure S32: Top (a) and side (b) views of NQ on α-Al_2O_3 (0001) for binding mode flat, geometry #15